Transactions of the Materials Research Society of Japan 30[1] 47-50 (2005)

Effects of Sample Geometry on Electric-Field-Induced Displacements in Pt/PZT/Pt/SiO_2/Si System Investigated by Finite Element Method

Hirotake Okino, Kazuo Nakamura, Hirofumi Matsuda[1], Takashi Iijima[2], Shintaro Yokoyama[3], Hiroshi Funakubo[3] and Takashi Yamamoto

Department of Communications Engineering, National Defense Academy, 1-10-20 Hashirimizu, Yokosuka, Kanagawa 239-8686, Japan
Fax: +81-468-44-5911, E-mail: hokino@nda.ac.jp
[1]Energy Technology Research Institute, National Institute of Advanced Industrial Science and Technology, 1-1-1 Umezono, Tsukuba, Ibaraki 305-8568, Japan
[2]Research Institute of Instrumentation Frontier, National Institute of Advanced Industrial Science and Technology, 1-1-1 Umezono, Tsukuba, Ibaraki 305-8568, Japan
[3]Department of Innovative and Engineered Materials, Tokyo Institute of Technology, 4259 Nagatsuta, Midori-ku, Yokohama, Kanagawa 226-8502, Japan

Electric-field-induced displacements of PZT film capacitor Pt/PZT/Pt/SiO_2/Si(100) were calculated by finite element method with various parameters of sample geometry. Sample geometric parameters were the diameter of top electrode ϕ_{TE} ranging from 0.2 μm to 1000 μm, PZT film thickness t_{PZT} ranging from 0.5 μm to 10 μm and whether PZT film was continuous or side-etched. The thickness of the substrate (SiO_2/Si(100)) t_{sub} was 300 μm. Surface longitudinal displacements and net longitudinal displacements of the PZT film were computed out, which corresponded to strains measured using an atomic force microscope (AFM) and a double beam interferometer (DBI), respectively. Five types of effects that prevent measurement of the intrinsic d_{33} using AFM were clarified. For measurement of the intrinsic d_{33}, both smaller ϕ_{TE} (less than t_{PZT}) and side-etch treatment were essential; however this condition is difficult to be satisfied experimentally. Thus, the second best condition was suggested.

Key words: piezoelectric thin films, electric-field-induced displacements, longitudinal piezoelectric constant, finite element method

1 INTRODUCTION

In case of materials research for ferroelectric micro electromechanical systems (MEMS), it has been important to measure electric-field-induced displacements and to evaluate piezoelectric constants (particularly longitudinal piezoelectric constant d_{33}) of ferroelectric films. Currently, several techniques such as atomic force microscopy (AFM)[1-5], interferometry[6-8] and direct methods[9] have been employed to evaluate the electric-field-induced displacements. The double-beam interferometer[6] has been the most precision technique; however it has needed a well-skilled operator and some sample processing. Thus, among these techniques, AFM has been the most effective technique for materials research, because AFM is easy to operate and has sufficient sensitivity.

Nevertheless, there has been some doubt whether piezoelectric constant d_{33} evaluated from AFM-measured strain has been intrinsic d_{33} or not. For instance, AFM-measured d_{33} has depended on the diameter of top electrode[5]. Moreover, in general, reported values of effective d_{33} have widely dispersed.

In this study, we calculated electric-field-induced displacements of PZT film capacitor by finite element method (FEM) and evaluated d_{33} with various parameters of sample geometry. Five types of effects which prevent precision measurement of d_{33} using AFM will be discussed.

2 THE SIMULATION MODEL

3-dimensional FEM analyses were performed using a commercial software (Dynus Co. Ltd., PiezoPLUS). Electric-field-induced displacements were calculated using static analysis mode, because applied field frequencies for AFM measurements (Hz $\sim$ kHz) are sufficiently lower than the mechanical resonance frequencies of thin film capacitore disks ($>$MHz). Columnar FEM models consisted of 5 layers as shown in Fig. 1: Pt/PZT/Pt/SiO_2/Si(100). These models had three parameters. First parameter was the diameter of the top electrode (ϕ_{TE}), which was ranging from 0.2 μm to 1,000 μm. Second parameter was the thickness of the PZT layer (t_{PZT}), which was ranging from 0.5 μm to 10 μm. Third parameter

Table 1 Summary of FEM model structure.

component	diameter (μm)	thickness (μm)	num. of elements along thickness
Pt top-electrode	ϕ_t = 0.2, 0.5, 1, 2, 5, 10, 20, 50, 100, 200, 500, 1000	0.1	5
PZT(52/48)	$\phi_t \times 1$ (for side-etched model) $\phi_t \times 10$ (for non-side-etched model)	0.5, 1, 2, 5, 10	20
Pt bottom electrode	$\phi_t \times 10$	0.1	5
SiO_2	$\phi_t \times 10$	1	10
Si single crystal	$\phi_t \times 10$	299	25

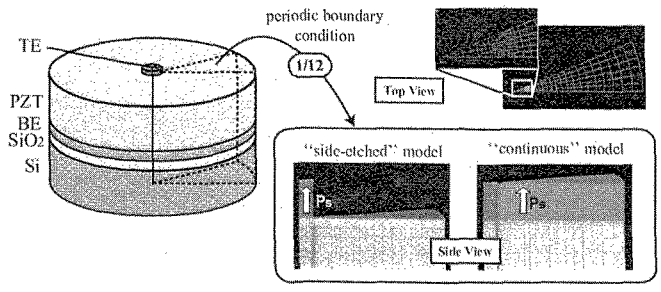

Fig. 1 Schematic drawings of FEM models.

Table 2 Mechanical properties of non-piezoelectric materials for FEM calculations.

	d	E	σ
Pt	21.44 [10]	0.168 [11]	0.377 [11]
SiO_2	2.20 [12]	0.073 [12]	0.165 [12]
Si	2.33 [13]	0.127 [14]	0.278 [14]

d: density (10^3 kg/m^3)
E: Young's modulus (10^{12} N/m^2)
σ: Poisson's ratio

was "whether PZT film was continuous or side-etched". The diameters of the whole FEM models were 10 times as large as ϕ_{TE}. As a mechanical boundary condition, the side faces of the models were clamped. A periodic boundary condition was applied in the rotation direction with a period of 30 ° so as to reduce computing time and to achieve more fine meshes. The parameters of the model structure are summarized in table 1.

Piezoelectric constants (d_{ij}^T), compliances (s_{ij}^E), permittivities (ε_{ij}^T) and density of pure PZT(52/48) ceramics[15] were substituted for these constants of the PZT film. Here, d_{33} of PZT was 223×10^{-12} m/V[15]. The mechanical constants of other materials are summarized in table 2. After the FEM calculations, $d_{33(AFM)}$ was computed from a longitudinal displacement at the center of the top-electrode surface. This value corresponds to d_{33} estimated from AFM-measured strain. $d_{33(net)}$ was also calculated from PZT film deformation in the film thickness direction on the center axis of the model. This value corresponds to d_{33} estimated from a longitudinal strain measured by the double-beam interferometer.

3 RESULTS AND DISCUSSION

Figure 2 shows the subtraction of $d_{33(AFM)}$ from $d_{33(net)}$ as a function of ϕ_{TE}, which was calculated with the side-etched models with various t_{PZT}. The result for the continuous models was almost the same with it. If ϕ_{TE} was equal to t_{PZT} or below, $d_{33(net)} - d_{33(AFM)}$ was nearly zero, indicating that AFM-measured d_{33} is similar to DBI-measured d_{33} on this condition. With increasing ϕ_{TE} from t_{PZT}, $d_{33(net)} - d_{33(AFM)}$ rose to a stationary value of approximately 50×10^{-12} m/V ($t_{PZT} < \phi_{TE} < 20 \times t_{PZT}$), kept the constant value ($20 \times t_{PZT} < \phi_{TE} < 200\,\mu$m), and rose rapidly again ($200\,\mu\text{m} < \phi_{TE}$). Thus, the dependences of $d_{33(net)} - d_{33(AFM)}$ in ϕ_{TE} were distinguished by four regions with three boundary: $\phi_{TE} = t_{PZT}$, $\phi_{TE} = 20 \times t_{PZT}$ and $\phi_{TE} = 200\,\mu$m. Here, it should be noted that the boundary, $\phi_{TE} = 200\,\mu$m, was independent of the PZT thickness, while other two boundaries were proportional to ϕ_{TE}. The additional calculations with a parameter of the substrate thickness t_{sub} pointed out that this boundary depended on the aspect ratio of ϕ_{TE} to t_{sub} and was around $\phi_{TE} = 0.5 \times t_{sub}$.

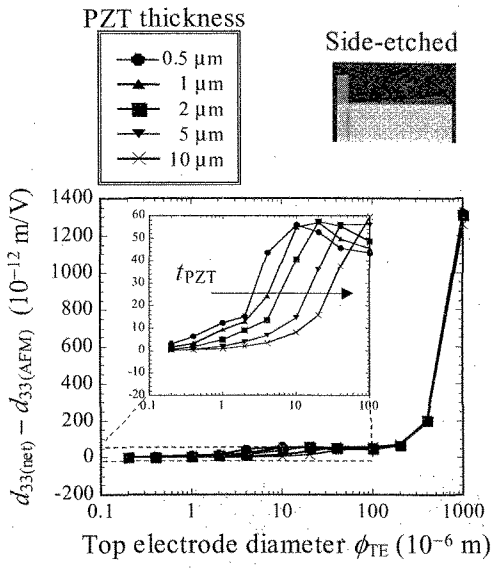

Fig. 2 Subtraction of AFM-measured d_{33} ($d_{33(AFM)}$) from DBI-measured d_{33} ($d_{33(net)}$) as a function of the diameter of the top electrode (ϕ_{TE}), which was calculated with the side-etched models with various t_{PZT}.

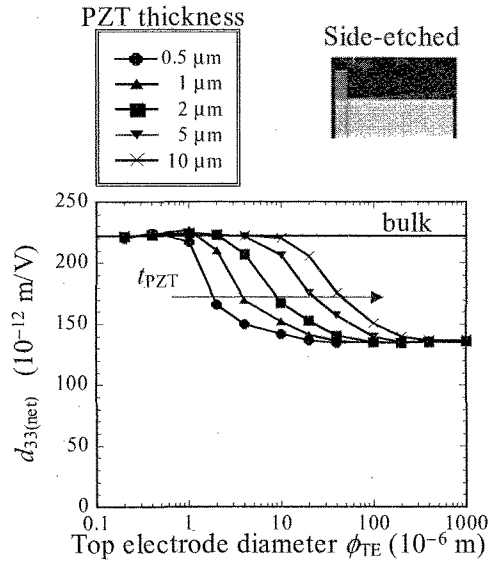

Fig. 3 DBI-measured d_{33} ($d_{33(net)}$) as a function of the diameter of the top electrode (ϕ_{TE}), which was calculated with the side-etched models with various t_{PZT}.

From detailed inspection of the sample deformations, it was found that the rapid increase of $d_{33(net)} - d_{33(AFM)}$ with ϕ_{TE} over 200 μm was attributed to a substrate bending effect: substrate bending motion due to a lateral piezoelectric effect, which has been reported by A. L. Kholkine *et al* [6]. If the aspect ratio of the top-electrode diameter to the substrate thickness is too large, a vertical displacement caused by the substrate-bending motion is not negligible. Thus, in a range of large ϕ_{TE} ($> 0.5 \times t_{sub}$), the displacement measured by AFM is dominated by the surface bending motion and $d_{33(AFM)}$ no longer correspond to the intrinsic d_{33}. It must be noted that the false displacement due to the substrate-bending effect strongly depended on mechanical boundary conditions for the FEM simulation. This implied that AFM-measured longitudinal strain easily changes with sample holding conditions, if ϕ_{TE} is large. The substrate-bending displacement is negligible, if ϕ_{TE} is reduced enough or if the field-induced displacement is measured by DBI.

The investigation of the sample deformations also revealed that the stationary difference between $d_{33(AFM)}$ and $d_{33(net)}$, which was found on the condition of $20 \times t_{PZT} < \phi_{TE} < 200\,\mu$m, was due to local backside displacement of the PZT capacitor. If there is no substrate and the PZT capacitor is totally free, the backside displacement is equal to the surface one. The asymmetry between the surface displacement and the backside one was attributable to the existence of the substrate. As described above, if ϕ_{TE} was small below t_{PZT}, $d_{33(AFM)}$ was almost equal to $d_{33(net)}$, implying that the backside displacement was negligible. This is because the substrate was able to be regarded as a perfect rigid body, if ϕ_{TE} was small enough.

Figure 3 shows $d_{33(net)}$ as a function of ϕ_{TE} calculated with the side-etched models with various t_{PZT}. If ϕ_{TE} was equal to t_{PZT} or below, $d_{33(net)}$ was equivalent to the bulk value: $d_{33}^{bulk} = 223 \times 10^{-12}$ m/V. As ϕ_{TE} increased from t_{PZT}, $d_{33(net)}$ declined and finally reached a stationary value of around 140×10^{-12} m/V independent of the PZT thickness. This stationary value was obtained if ϕ_{TE} was larger than $20 \times t_{PZT}$.

This difference between d_{33}^{bulk} and $d_{33(net)}$ was caused by a clamping in the lateral directions by the substrate.[16] It has also been reported that the stationary d_{33} value, in this case 140×10^{-12} m/V, depends on both d_{31} and the Poisson's ratio of the piezoelectric film in principle.[16] This in-plane clamping effect is negligible, if the aspect ratio of ϕ_{TE} to t_{PZT} is 1 or less.

Figure 4 shows the subtraction of $d_{33(net)}$ for the continuous models from $d_{33(net)}$ for the side-etched models as a function of ϕ_{TE}, which was calculated with various t_{PZT}. This subtraction represents the effectiveness of the side-etch treatment. If ϕ_{TE} was larger than $20 \times t_{PZT}$, $d_{33(net)}^{cont.} - d_{33(net)}^{etched}$ was almost zero, indicating that the side-etch treatment has no effect on this condition. As ϕ_{TE} decreased, $d_{33(net)}^{cont.} - d_{33(net)}^{etched}$ gradually increased,

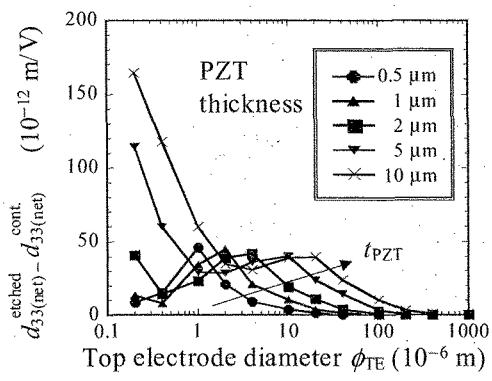

Fig. 4 Subtraction of DBI-measured d_{33} ($d_{33(\mathrm{net})}$) for the continuous models from $d_{33(\mathrm{net})}$ for the side-etched models as a function of the diameter of the top electrode (ϕ_{TE}).

exhibited local maximal values at $\phi_{TE} = 2 \times t_{PZT}$, and finally rose drastically ($\phi_{TE} < 0.5 \times t_{PZT}$).

A detailed investigation of the sample deformations revealed that the drastic increase of $d_{33(\mathrm{net})}^{\mathrm{cont.}} - d_{33(\mathrm{net})}^{\mathrm{etched}}$ with decreasing ϕ_{TE} below $0.5 \times t_{PZT}$ was due to an edge-clamping effect: the continuous PZT film clamped the edge of the capacitor disk and prevented the whole disk from elongating longitudinally. In case of side-etched model, the capacitor disk was deformed almost freely, because of the absence of the continuous PZT film. Thus, the side-etch treatment is essential if ϕ_{TE} is smaller than $0.5 \times t_{PZT}$.

The sample deformation also clarified that an in-plane clamping caused by the continuous PZT layer was the origin of the difference between $d_{33(\mathrm{net})}^{\mathrm{cont.}}$ and $d_{33(\mathrm{net})}^{\mathrm{etched}}$ observed on the condition of $\phi_{TE} > 0.5 \times t_{PZT}$ with the local maxima. The side-etch treatment also eliminate this effect.

4 CONCLUSIONS

Electric-field-induced displacements of PZT film capacitor Pt/PZT/Pt/SiO2/Si(100) were calculated by finite element method with various parameters of sample geometry. Five effects which prevented precision measurement of d_{33} using AFM were clarified by FEM calculations: (1) the substrate-bending effect ($0.5 \times t_{sub} < \phi_{TE}$), (2) the local backside displacement ($t_{PZT} < \phi_{TE}$; const. if $20 \times t_{PZT} < \phi_{TE}$), (3) the in-plane clamping by the substrate ($t_{PZT} < \phi_{TE}$; const. if $20 \times t_{PZT} < \phi_{TE}$), (4) the in-plane clamping by the continuous film ($\phi_{TE} < 20 \times t_{PZT}$) and (5) the edge-clamping effect ($\phi_{TE} < 0.5 \times t_{PZT}$). The substrate-bending effect and the local backside displacement were negligible, if the displacements were measured by DBI. The side-etch treatment were effective to eliminate the in-plane clamping by the continuous film and the edge-clamping effect.

For measurement of the intrinsic d_{33}, both smaller ϕ_{TE} (less than t_{PZT}) and side-etch treatment were essential; however this condition is difficult to be satisfied experimentally. Thus, the second best condition, $20 \times t_{PZT} < \phi_{TE} < 0.5 \times t_{sub}$ was suggested. On the second best condition, AFM-measured displacements depended only on d_{31} and Poisson's ratio of PZT and was relatively independent of sample geometric parameters, particularly ϕ_{TE}.

Acknowledgements

This work was partly supported by the Nissan Science Foundation.

REFERENCES

[1] H. Maiwa, J.-P. Maria, J. A. Christman, S.-H. Kim, S. K. Streiffer, and A. I. Kingon, Integr. Ferroelectr. **24**, 139 (1999).
[2] H. Maiwa and N. Ichinose, Jpn. J. Appl. Phys **39**, 5403 (2000).
[3] S. Bühlmann, B. Dwir, J. Baborowski, and P. Muralt, Appl. Phys. Lett. **80**, 3195 (2002).
[4] V. Nagarajan et al., Appl. Phys. Lett. **81**, 4215 (2002).
[5] T. Iijima, S. Ito, and H. Matsuda, Jpn. J. Appl. Phys. **41**, 6735 (2002).
[6] A. L. Kholkine, C. Wüetchrich, D. V. Taylor, and N. Setter, Rev. Sci. Instrum. **67**, 1935 (1996).
[7] T. Iijima, Y. Hayashi, and J. Onagawa, Mater. Res. Soc. Symp. Proc. **688**, 343 (2002).
[8] T. Iijima and K. Kunii, Jpn. J. Appl. Phys. **40**, 5740 (2001).
[9] F. Xu, F. Chu, J. F. Shepard Jr., and S. Troiler-McKinstry, Mater. Res. Soc. Symp. Proc. **493**, 427 (1998).
[10] J. F. Shackelford and W. Alexander, *CRC Materials Science and Engineering Handbook*, page 48, CRC Press, Boca Raton, 2000.
[11] N. A. O. of Japan, *Rikanenpyou (in Japanese)*, chapter Physics, page 24, Maruzen, Tokyo, 1999.
[12] S. Spinner, J. Am. Ceram. Soc. **39**, 113 (1956).
[13] J. F. Shackelford and W. Alexander, *CRC Materials Science and Engineering Handbook*, page 46, CRC Press, Boca Raton, 2000.
[14] L. Gan, B. Ben-Nissan, and A. Ben-David, Thin Solid Films **290-291**, 362 (1996).
[15] D. A. Berlincourt, C. Cmolik, and H. Jaffe, Proc. of Inst. Radio Eng. **48**, 220 (1960).
[16] K. Lefki and G. J. M. Dormans, J. Appl. Phys. **76**, 1764 (1994).

(Received December 23, 2004; Accepted January 31, 2005)